Eur. J. Mineral.
2001, **13**, 497–505

This paper was presented at the EMPG VIII meeting in Bergamo, Italy (April 2000)

High-pressure structural behaviour of heulandite

PAOLA COMODI*, GIACOMO DIEGO GATTA and PIER FRANCESCO ZANAZZI

Dipartimento di Scienze della Terra, Università di Perugia, Piazza Università, I-06100 Perugia, Italy
* e-mail: comodip@unipg.it

Abstract: The structural evolution up to 5 GPa of a natural heulandite was studied using *in situ* single-crystal X-ray diffraction data from a diamond-anvil cell (DAC) with glycerol as the pressure transmitting medium. Linear regressions yielded mean axial compressibilities for *a*, *b* and *c* axes of $\beta_a = 1.02(1)\cdot10^{-2}$, $\beta_b = 8.1(6)\cdot10^{-3}$, $\beta_c = 7.6(2)\cdot10^{-3}$ GPa^{-1}. The largest strain vector ($\beta_1 = 1.16\ 10^{-2}$ GPa^{-1}) lies approximately on the diagonal of the system of channels along [100] and [001].

V_0, K_0, and K_0' refined with a third-order Birch-Murnaghan equation are: $V_0 = 2121(2)$ Å^3, $K_0 = 26.4(1.0)$ GPa, $K_0' = 4.9(8)$. If fitted with second-order Birch-Murnaghan equation of state, fixing $K_0' = 4$, K_0 becomes 27.5(2) GPa.

The bulk heulandite structure compression was the result of the "soft" behaviour of the channels (K=10-19 GPa) and the more rigid behaviour of the tetrahedral framework (K ≅ 60 GPa), which underwent tilting of the fundamental polyhedral unit (FPU) chains. The T5-T5-T5 angles, between the FPUs, decreased from 162.4° at 0.0001 GPa to 156.2° at 3.4 GPa.

The position of extra-framework cations and water molecules was almost maintained within the investigated pressure range. Up to 3.7 GPa no phase transition was observed. Amorphization was clearly observed at pressure above 4 GPa. The transition to the amorphous phase was still reversible up to 5 GPa.

Key-words: zeolite, heulandite, single-crystal X-ray diffraction, high pressure, compressibility.

Introduction

In recent years zeolite minerals have found increasing applications in many industrial fields (*e.g.*, pollution control, petroleum production, agricultural application). While the vast possibilities of exchanging cations and molecules, the catalytic ability and the structural thermal stability of this type of mineral have been investigated extensively, studies of their structural behaviour under pressure are scarce.

Hazen & Finger (1984) were the first to study the effect of hydrostatic pressure media on the compressibility of a synthetic zeolite 4A: ethanol, methanol, glycerol and organo-fluorine compound. They showed that the compressibility of this zeolite depends on the relative size of the hydrostatic-fluid molecules compared with the structural channels in the zeolite framework. Later Belitsky *et al.* (1992) studied the structural transformations induced by pressure in natrolite and edingtonite using liquids with various molecular dimensions as pressure-transmitting media. Their spectroscopic and diffractometric data showed that under high water pressures, some additional H_2O molecules entered the framework channels and caused an anisotropic swelling of the crystal and two phase transitions (natrolite II, natrolite III). If non-penetrating liquid was used no phase transitions were detected up to 7 GPa. In both cases it was observed that the transformations were completely reversible at least up to 7 GPa.

Gillet *et al.* (1996) studied pressure-induced amorphization on scolecite and mesolite by X-ray powder diffraction and Raman spectroscopy. In a non-penetrating pressure medium (KBr) these zeo-

0935-1221/01/0013-0497 $ 2.25
DOI: 10.1127/0935-1221/2001/0013-0497

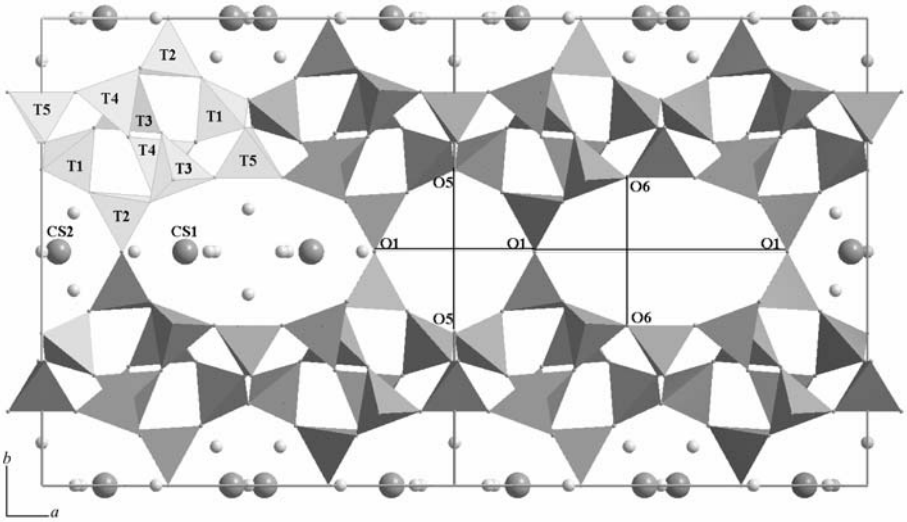

Fig. 1. Projection of heulandite structure along [001], showing the FPU, and along [100]. The three channels, with the "free diameters" and the extra-framework population are shown. The large spheres represent cation sites, whereas the small spheres represent the oxygen of the water molecules.

lites showed amorphous-phase transition at 8-9 GPa. The transitions from the crystal to the amorphous phase were irreversible, but in some scolecite experiments during decompression, below 7 GPa, the amorphized samples showed a crystalline rim of back-transformed phase. Similar evidence of recrystallisation after H*P*-amorphization has been observed in α-$AlPO_4$ (Gillet *et al*., 1995).

All of the quoted studies on natural fibrous zeolites (natrolite, edingtonite, scolecite and mesolite) were aimed at studying the H*P*-behaviour using X-ray powder diffraction but did not report structural data. No single-crystal H*P* structural data are available for other natural zeolites, yet there are many single-crystal H*T*-structural studies (Alberti & Vezzalini, 1984, and references therein; Vezzalini *et al*., 1993; Alberti *et al*., 1994).

The aim of our study was to investigate the structural evolution of heulandite under pressure using *in situ* X-ray single-crystal diffraction.

Heulandite is a common mineral in post-volcanic environments and belongs to the heulandite-clinoptilolite zeolite group. In his general scheme of zeolitic crystallisation during diagenesis and very low metamorphism, Utada (1970) attributed heulandite to "zone III" of "zeolite facies". Surface genesis has never been ascribed to this kind of zeolite, whereas it has been suggested for the isotypic framework of clinoptilolite.

The ion-exchange specificity of heulandite-clinoptilolite has been demonstrated very active in removing of radioactive Cs^{137} and Sr^{90} from low-level waste streams of nuclear installations and in extracting of ammonium from sewage (Smyth, 1982; Mumpton, 1988; Vaniman & Bish, 1993). Moreover, this natural zeolite is not only considerably less expensive than organic ion-exchange resins, it is also much more resistant to nuclear degradation. A high-pressure study of a nuclear waste disposal phase may be important both to determine the stability conditions and to evaluate how its exchange characteristics are modified by pressure, as well as to verify whether phase transitions occur or not.

The heulandite type framework is built from the "Fundamental Polyhedral Unit" (FPU, also called "secondary building unit"-SBU) depicted schematically in Fig. 1. The FPUs are first joined through the T5 atoms to form long chains along [102] with T5-T5-T5 angle equal to about 162° in natural heulandite. These chains are linked laterally through the T1, T3, T4 atoms to produce dense silicate layers (010). Parallel layers are joined through the T2 atoms to form a three-dimensional framework enclosing three systems of channels: 10-ring and 8-ring channels along [001], 8-ring channels along [100]. The extra-framework cations (CS1 and CS2) and water molecules lie in these channels. According to Bresciani-Pahor *et al.* (1980) the CS1 site is

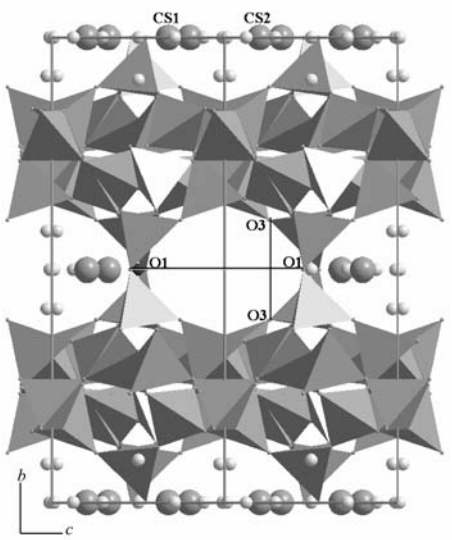

Fig. 1. (cont.)

occupied preferentially by monovalent cations and the CS2 site is occupied by Ca only, the residual bivalent cations (Ca, Sr, Ba) being in CS1. With these cation distributions, CS1 and CS2 have variable occupancies (Alberti, 1972; Alberti & Vezzalini, 1983). The extra-framework sites containing water molecules may also have variable occupancies. Their occupancies in heulandite-group zeolite may vary from one specimen to another and depend on bulk chemical composition. However, different studies have shown almost full occupancy for W3 and W4 sites regardless of the change in chemical composition (Alberti, 1972; Alberti & Vezzalini, 1983).

Alberti (1973) and Alberti & Vezzalini (1983) studied the structural behaviour of heulandite dehydration by X-ray single-crystal diffraction. They showed the heat-induced polymorphic transition (heulandite A - heulandite B) with the structural transformation produced by dehydration: strong deformation of the FPU, pronounced zig-zag of their chains along [102] and extra-framework site shifts. Mortier & Pearce (1981) studied the intermediate phase, called d-Ca/H-HEU, between the hydrated NH_4-exchanged heulandite and dehydrated heulandite B by X-ray single-crystal diffraction. They showed the structural differences for the activated (partially dehydrated) intermediate phase, stable at 483 K.

In our study this information on the behaviour of heulandite under pressure will be compared with the dehydration effect of heating. The amorphization process will also be examined, and on the basis of H*P* structural refinements, a tentative amorphization path of this zeolite will be proposed.

Experimental procedure

The heulandite specimen came from Paterson (New Jersey, U.S.A). The chemical composition, determined with an ARL-SEMQ microprobe (operating conditions: 15 kV, 10 nA measured on brass, beam size 30 µm, 20 s of counting time) and the water content measured with thermogravimetric analysis, using SEIKO SSC/5200 apparatus (in air, heating rate 10°C/min) at the "Dipartimento di Scienze della Terra" of Modena University, yielded the following chemical formula: $Na_{1.72}K_{0.40}Ca_{2.65}Ba_{0.03}Sr_{0.87}Al_{9.29}Si_{26.73}O_{72}$ $26.85H_2O$.

A Merrill-Bassett diamond anvil cell (DAC) with 1/8 carat diamond with 800 µm culet face diameter was used for high-pressure study. Steel Inconel 750X foil, 250 µm thick, with a 350 µm hole, was used as gasket material. A Sm^{2+}-BaFCl powder for pressure calibration (Comodi & Zanazzi, 1993) and glycerol ($C_3O_3H_6$) as pressure-transmitting medium were introduced into the DAC together with the sample. Glycerol was chosen because its large dimension molecules do not enter in the zeolite framework channels (Hazen & Finger, 1984).

Pressure was calculated by measuring the wavelength shift of the Sm^{2+} line (λ = 6876 Å, at 0.0001 GPa) excited by a 100 mW argon laser and detected by a 100 cm Jarrell-Ash optical spectrometer. The precision of pressure measurements was 0.05 GPa.

The lattice parameters of a crystal, with dimensions of 0.25 x 0.2 x 0.05 mm, were determined at various pressures between 0.0001 and 3.7 GPa (Table 1) by applying the least-square method to the Bragg angles of 36 accurately centred reflections.

Table 1. Lattice parameters and volumes of heulandite at different pressures.

P (GPa)	*a* (Å)	*b* (Å)	*c* (Å)	*β* (°)	*V* (Å^3)
0.0001	17.729(1)	17.909(4)	7.433(2)	116.52(2)	2111.7(4)
0.24	17.701(6)	17.791(5)	7.405(7)	116.45(5)	2089.3(5)
0.89	17.592(7)	17.711(4)	7.380(8)	116.58(7)	2054.2(2)
1.45	17.481(6)	17.625(7)	7.345(5)	116.73(8)	2021.5(3)
2.07	17.347(8)	17.507(6)	7.305(6)	116.80(7)	1980.6(4)
2.76	17.235(5)	17.445(8)	7.274(8)	116.83(9)	1952.3(4)
3.40	17.124(6)	17.376(7)	7.237(7)	116.93(8)	1920.2(6)
3.72	17.072(6)	17.331(7)	7.215(7)	117.10(8)	1901.4(3)
0.0001*	17.774(2)	17.824(3)	7.438(3)	116.38(2)	2110.9(5)

* data collected under room conditions after compression.

Table 2. Some details of data collection and refinements of heulandite.

Pressure (GPa)	0.0001	1.45	3.4	0.0001*
Radiation	Mo*K*α	Mo*K*α	Mo*K*α	Mo*K*α
θ range (°)	3÷35	3÷35	3÷35	3÷35
Scan type	ω	ω	ω	ω
Scan speed (°/s)	0.06	0.06	0.06	0.08
Scan width (°)	1.8	2.6	2.6	2.6
Space group	*C*2/*m*	*C*2/*m*	*C*2/*m*	*C*2/*m*
No. Measured refl.	4417	1055	1224	4670
No. Independent refl.	2804	600	686	2999
No. Observed refl.	1353	241	268	1529
No. Parameters	178	79	79	178
R_{eq}	4.16	12.12	14.40	3.55
R %	4.67	7.04	7.75	4.88

* data collected under room conditions after compression.

Diffraction data were collected under room conditions on a Philips PW 1100 four-circle diffractometer using a graphite monochromator for Mo*K*α radiation (λ = 0.7107 Å); ω scanned with scan width 1.8° and scan speed 0.06°/s were employed. 2804 independent reflections were collected for the structural refinement (Table 2). Empirical absorption correction based on the method of North *et al*. (1968) was applied and 1353 observed reflections with intensities higher than 3σ(I) were employed. The refinement was carried out with anisotropic displacement parameters in space group *C*2/*m* using the SHELX-97 program (Sheldrick, 1997). The final agreement index was 4.67 % for 178 parameters. The neutral atomic scattering factor values from the *International Tables for X-ray Crystallography* (Ibers & Hamilton, 1974) were used. Whereas for CS2 a scattering curve of calcium alone was used, for CS1 site a mixed curve built with the scattering curves of Na, K, Sr, Ba and Ca, in percentages consistent with the analysis, were employed.

The intensity data were collected at 1.4 and 3.4 GPa up to 35° of θ, adopting non-bisecting geometry (Denner *et al*., 1978) and 2.6° ω scans; when possible, the measurements were repeated at different azimutal ψ angles. Data were corrected for pressure-cell absorption with an experimental attenuation curve (Finger & King, 1978).

The H*P* structures were refined with isotropic atomic displacement parameters and site occupancies fixed to the room condition value. Details of the refinements are listed in Table 2. Observed and calculated structure factors can be obtained from the authors upon request (or through the E.J.M. Editorial Office – Paris).

Results

Results under room conditions

The heulandite structure was refined with starting coordinates from Alberti (1972). The coordinates of the framework atoms are very close to those found by Alberti & Vezzalini (1983) for heulandite from Nadap and for heulandite from Azerbaijan (Bresciari-Pahor *et al*., 1980).

Special care was devoted to the location of the extra-framework cations and water molecules. We found six sites for the water molecules, some completely occupied and others partially occupied (Table 3). The seventh (W7) water site, found partially occupied in Nadap heulandite (Alberti & Vezzalini, 1983), was completely empty in this sample.

The determination of Al-content in the tetrahedra was carried out using Alberti's method (Alberti & Gottardi, 1988). The result was: T1(Al)= 19.2 %, T2(Al) = 36.3 %, T3(Al) = 19.9 %, T4(Al) = 19.4 %, T5(Al) = 33.4 %, with Al-content total equal to 8.92 atoms per formula unit (a.f.u.). This result is in good agreement with chemical data from the analysis. On the other hand by applying Jones' method (Jones, 1968) the result was: T1(Al) = 19.6 %, T2(Al) = 33.7 %, T3(Al) = 16.8 %, T4(Al) = 14.0 %, T5(Al) = 31.4 %, with Al-content total equal to 7.98 a.f.u.

Compressibility

The reduction of lattice parameters with pressure was linear, without evidence of phase transitions in the pressure range investigated. Linear regressions (Fig. 2) yielded mean axial compressibilities for *a*, *b* and *c* axes of $\beta_a = 1.02(1)\cdot10^{-2}$, $\beta_b = 8.1(6)\cdot10^{-3}$, $\beta_c = 7.6(2)\cdot10^{-3}$ GPa^{-1}. As shown in Fig. 2, the β angle increased slightly with pressure.

The principal linear compression coefficients are not constrained by symmetry to completely coincide with crystallographic axes. Thus, to determine the strain ellipsoid and its orientation with respect to the crystallographic axes, analysis of the strain tensor was performed using the program STRAIN (Ohashi, 1982). The principal axes of the strain tensor calculated between 0.0001 and 3.5 GPa, using the lattice parameter values obtained from linear regressions, were: $\beta_1 = 1.16\cdot10^{-2}$, $\beta_2 = 8.1\cdot10^{-3}$, $\beta_3 = 7.5\cdot10^{-3}$ GPa^{-1}. β_2 was coincident with the *b* axis, whereas β_1 and β_3 lie in the plane (010). β_1 formed an angle of about 35° with the *a* axis; this

Table 3. Atomic fractional coordinates, electron numbers and thermal displacement factors (Å^2).

Site	X	y	z	Σe$^-$	Uiso/Ueq
CS1	0.1523(2)	0.0	0.6735(6)	16.44	0.045(1)
	0.1503(8)	0.0	0.675(2)	16.44	0.043(5)
	0.1431(8)	0.0	0.673(2)	16.44	0.038(4)
	0.1543(2)	0.0	0.6757(5)	16.60	0.044(1)
CS2	0.0398(2)	0.5	0.2024(7)	9.44	0.033(1)
	0.033(1)	0.5	0.185(3)	9.44	0.028(6)
	0.027(2)	0.5	0.158(6)	9.44	0.09(1)
	0.0408(2)	0.5	0.2003(7)	9.20	0.028(1)
T1	0.1795(1)	0.1698(1)	0.0966(2)	13.81	0.0144(4)
	0.1818(4)	0.164(1)	0.101(1)	13.81	0.014(2)
	0.183(4)	0.166(1)	0.103(1)	13.81	0.013(2)
	0.1796(1)	0.1682(1)	0.0957(2)	13.81	0.0142(3)
T2	0.2109(1)	0.4098(1)	0.4988(2)	13.64	0.0150(4)
	0.2071(4)	0.409(2)	0.490(2)	13.64	0.019(2)
	0.2014(4)	0.415(1)	0.479(1)	13.64	0.014(2)
	0.2109(1)	0.4098(1)	0.4985(2)	13.64	0.0143(3)
T3	0.2084(1)	0.1903(1)	0.7174(2)	13.80	0.0145(4)
	0.2072(4)	0.189(1)	0.716(1)	13.80	0.012(2)
	0.2075(5)	0.189(1)	0.719(1)	13.80	0.017(2)
	0.2088(1)	0.1910(1)	0.7183(2)	13.80	0.0138(3)
T4	0.0645(1)	0.2978(1)	0.4100(2)	13.81	0.0146(4)
	0.0606(5)	0.295(1)	0.403(1)	13.81	0.018(2)
	0.0563(5)	0.293(1)	0.393(1)	13.81	0.017(2)
	0.0643(1)	0.2984(1)	0.4111(2)	13.81	0.0145(3)
T5	0.0	0.2126(1)	0.0	13.66	0.0154(5)
	0.0	0.205(2)	0.0	13.66	0.018(3)
	0.0	0.199(2)	0.0	13.66	0.019(3)
	0.0	0.2115(1)	0.0	13.66	0.0165(5)
O1	0.1940(5)	0.5	0.455(1)	16.00	0.029(2)
	0.191(2)	0.5	0.451(6)	16.00	0.04(1)
	0.168(3)	0.5	0.407(7)	16.00	0.06(1)
	0.1953(5)	0.5	0.450(1)	16.00	0.028(1)
O2	0.2317(3)	0.1190(1)	0.6143(8)	16.00	0.031(1)
	0.229(1)	0.120(3)	0.607(3)	16.00	0.020(6)
	0.227(1)	0.117(4)	0.612(4)	16.00	0.041(7)
	0.2316(3)	0.1206(3)	0.6116(7)	16.00	0.029(1)
O3	0.1829(3)	0.1533(3)	0.8849(7)	16.00	0.028(1)
	0.182(1)	0.144(3)	0.884(4)	16.00	0.031(7)
	0.179(1)	0.148(3)	0.887(3)	16.00	0.027(6)
	0.1854(3)	0.1524(3)	0.8855(7)	16.00	0.029(1)
O4	0.2388(3)	0.1068(3)	0.2567(7)	16.00	0.027(1)
	0.248(1)	0.105(3)	0.264(3)	16.00	0.020(6)
	0.256(1)	0.101(3)	0.264(3)	16.00	0.027(6)
	0.2403(3)	0.1059(3)	0.2566(6)	16.00	0.027(1)
O5	0.0	0.3252(5)	0.5	16.00	0.032(2)
	0.0	0.329(4)	0.5	16.00	0.029(9)
	0.0	0.338(5)	0.5	16.00	0.05(1)
	0.0	0.3266(4)	0.5	16.00	0.034(1)
O6	0.0821(2)	0.1579(3)	0.0642(7)	16.00	0.023(1)
	0.087(1)	0.146(3)	0.085(3)	16.00	0.027(7)
	0.088(1)	0.144(3)	0.096(3)	16.00	0.019(6)
	0.0833(3)	0.1558(3)	0.0626(7)	16.00	0.025(1)
O7	0.1272(3)	0.2349(3)	0.5483(8)	16.00	0.037(1)
	0.127(1)	0.240(4)	0.550(4)	16.00	0.045(7)
	0.120(1)	0.239(4)	0.548(4)	16.00	0.048(7)
	0.1271(3)	0.2348(3)	0.5542(8)	16.00	0.038(1)
O8	0.0084(3)	0.2659(3)	0.1841(7)	16.00	0.030(1)
	0.003(1)	0.261(3)	0.185(3)	16.00	0.029(7)
	–0.007(1)	0.248(3)	0.177(4)	16.00	0.031(6)
	0.0094(3)	0.2658(3)	0.1863(7)	16.00	0.035(1)
O9	0.2105(3)	0.2540(3)	0.1750(7)	16.00	0.029(1)
	0.207(1)	0.257(4)	0.170(4)	16.00	0.033(7)
	0.209(1)	0.252(3)	0.175(3)	16.00	0.016(5)
	0.2099(3)	0.2532(3)	0.1756(7)	16.00	0.027(1)
O10	0.1148(3)	0.3724(3)	0.3962(7)	16.00	0.026(1)
	0.112(1)	0.367(3)	0.376(3)	16.00	0.036(7)
	0.106(1)	0.359(3)	0.350(3)	16.00	0.033(7)
	0.1151(3)	0.3726(3)	0.3975(7)	16.00	0.028(1)
W1	0.2242(6)	0.5	–0.009(1)	16.00	0.052(2)
	0.223(2)	0.5	–0.003(5)	16.00	0.04(1)
	0.229(2)	0.5	0.005(5)	16.00	0.03(1)
	0.2223(6)	0.5	–0.009(1)	16.00	0.048(2)
W2	0.080(1)	0.0	0.880(3)	12.80	0.106(9)
	0.079(2)	0.0	0.875(7)	12.80	0.08(2)
	0.079(3)	0.0	0.884(9)	12.80	0.09(2)
	0.0795(8)	0.0	0.875(3)	14.72	0.111(8)
W3	0.0773(4)	0.4173(5)	0.970(1)	16.00	0.065(2)
	0.078(1)	0.408(3)	0.948(4)	16.00	0.06(1)
	0.088(2)	0.407(4)	0.942(5)	16.00	0.09(1)
	0.0769(4)	0.4172(5)	0.969(1)	16.00	0.062(2)
W4	0.0	0.5	0.5	16.00	0.077(5)
	0.0	0.5	0.5	16.00	0.07(2)
	0.0	0.5	0.5	16.00	0.09(2)
	0.0	0.5	0.5	16.00	0.074(5)
W5	0.0	0.091(1)	0.5	16.00	0.19(2)
	0.0	0.084(8)	0.5	16.00	0.21(4)
	0.0	0.093(6)	0.5	16.00	0.08(1)
	0.0	0.0909(9)	0.5	16.00	0.21(1)
W6	0.095(1)	0.0	0.288(3)	15.36	0.121(9)
	0.101(2)	0.0	0.321(7)	15.36	0.07(1)
	0.104(2)	0.0	0.319(6)	15.36	0.05(1)
	0.097(1)	0.0	0.291(3)	14.72	0.13(1)

Note: For each atom values from top to bottom correspond to the refinement at 0.0001, 1.45, 3.4 and 0.0001 (after decompression) GPa respectively. For each tetrahedral site, the Si/Al content is determined using Alberti's method. For H*P* refinements the isotropic thermal parameters, Uiso, are reported, whereas for the room condition refinements Ueq is shown.

direction roughly corresponds to the diagonal of the system of channels along [100] and [001] (Fig. 3).

Volume compression data, isothermal bulk modulus K_0 and its pressure derivative K_0', were fitted to a third-order Birch-Murnaghan equation of state (Birch, 1978). The equation has the form:

$$P = 3/2K_0[(V_0/V)^{7/3} - (V_0/V)^{5/3}]\{1 + 3/4(K_0' - 4)[(V_0/V)^{2/3} - 1]\}$$

and was solved using a Levenberg-Marquardt algorithm (Press *et al*., 1986).

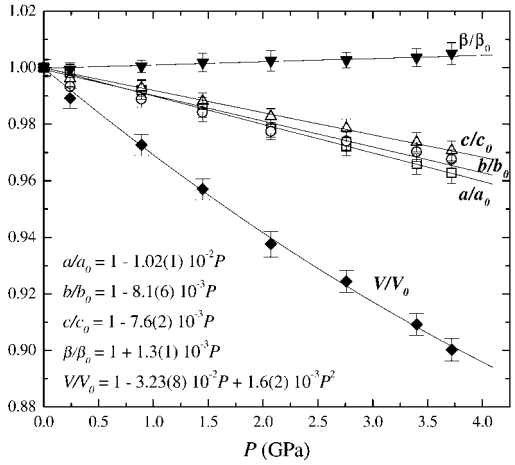

Fig. 2. Unit-cell parameters, normalised to room condition value, *vs.* pressure. The regression line equations are reported in the bottom left hand corner.

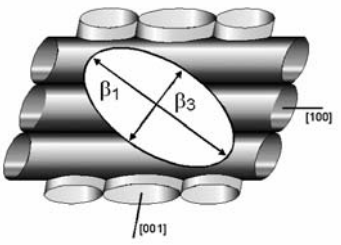

Fig. 3. Strain ellipsoid orientation and the channel system along [001] and [100].

When V_0, K_0, and K_0' were refined, the values obtained were : V_0 = 2121(2) Å^3, very close to the value measured under room conditions (Table 1), K_0 = 26.4(1.0) GPa, K_0' = 4.9(8). If the data were fitted to a second-order Birch-Murnaghan equation of state, with fixed K_0' = 4, K_0 became 27.5(2) GPa.

A subtle effect is observed in the heulandite compressibility: a slight deviation from the linear *V vs. P* trend may be observed. This effect may be described in terms of the following quadratic trend: $V/V_0 = 1 - 3.23(8)\cdot10^{-2}P + 1.6(2)\cdot10^{-3}P^2$.

The bulk modulus of heulandite, using a non-penetrating pressure medium, is similar to the bulk moduli of other open framework compounds, such as zeolite-4A with $K_0 \cong$ 21GPa (Hazen & Finger, 1984), but is significantly smaller than that observed in other framework silicates (*e.g.*, in analcite, K_0 = 41 GPa, Hazen & Finger, 1979; in marialite, K_0 = 60 GPa, Comodi *et al*., 1990; in anorthite, K_0 = 94 GPa, Angel *et al.*, 1988).

Structural evolution with pressure

The H*P* structural behaviour of this zeolite type was studied by comparing the three refinements carried out at 0.0001, 1.45 and 3.4 GPa. The pressure increase did not produce relevant variations in the tetrahedral bond distances (Table 5) as observed in most silicates in this pressure range. On the other hand, as expected for open framework structures, the main deformation mechanism was the polyhedral tilting that produced inter-tetrahedral angle variations. In particular in heulandite the most relevant variation produced by polyhedral tilting was the shortening of the zig-zag chain, along [102], formed by the heulandite polyhedral unit (FPU). The T5-T5-T5 angles between the FPUs decreased from 162.4(1)° at 0.0001 GPa to 156.2(3)° at 3.4 GPa (Table 4). At the same time the 8- and 10-membered ring channels parallel to *c* were compressed, principally along [010]. The channel bulk moduli, calculated from the volume variations of the inscribed elliptical-section cylinders, were quite low: the bulk moduli of the 10- and 8- membered ring channels along [001] were 19(2) and 10(2.3) GPa respectively. That of 8-membered ring channels along [100] was 18(1.5) GPa (Table 4).

Tetrahedral tilting not only changed the configuration between the FPUs, but also the size of the FPU itself. The FPU "pseudo-volume", defined as the product of the three distances (T2-T2), (T3-T3), (T5-T5) across the FPU (Mortier & Pearce, 1981), changed from 244.5(3) Å^3 under room conditions to 230.9(4) Å^3 at 3.4 GPa. Thus the FPU bulk modulus was 63(8) GPa (Table 4).

Besides relevant decrease in the channel free volumes, the pressure increase induced important variations in the shape of the channels. We can evaluate the evolution on the channel ellipticity by the ratio between the smaller free diameter compared to the larger one, O6-O6/O1-O1 for the 10-ring channel, O5-O5/O1-O1 for the 8-ring channel along [001], O3-O3/O1-O1 for the 8-ring channel along [100]. According to the results shown in Table 4, it appears that whereas the shape of the 8-ring channels did not change much with pressure, the 10-ring channel became more elliptic. The ratio O6-O6/O1-O1 changed from 0.38 to 0.28 with pressure increase of 3.4 GPa, corresponding to a decrease of about 26 %, while in the 8-ring channels the ellipticity decreases were 3 and 9 %. Due to the 10-ring channel compressing along [010], the O1 oxygen moves towards the inside of the 8-ring channel, as indicated from the atomic coordinates (Table 3).

Table 4. Relevant structural parameters in heulandite at different pressures.

P (GPa)	0.0001	1.45	3.40	0.0001*	K (GPa)
Vol- FPU (Å^3)	244.5(3)	234.0(2)	230.9(4)	238.3(3)	63(8)
T5-T5-T5 (°)	162.4(1)	159.1(3)	156.2(3)	162.0(2)	
T5-T5 (Å)	8.965(5)	8.664(7)	8.525(8)	8.801(4)	
Channel [001]					
O1-O1$_{10\text{-ring}}$ (Å)	7.86(3)	7.78(4)	8.11(3)	7.82(2)	
O6-O6$_{10\text{-ring}}$ (Å)	2.95(1)	2.38(7)	2.31(5)	2.85(3)	
O1-O1$_{8\text{-ring}}$ (Å)	4.50(4)	4.35(5)	3.80(4)	4.60(2)	
O5-O5$_{8\text{-ring}}$ (Å)	3.56(6)	3.40(3)	2.91(4)	3.48(4)	
$V_{ch10\text{-ring}}$ (Å^3)	121.3(3)	110.4(5)	94.9(6)	116.7(4)	19(2)
$V_{ch\ 8\text{-ring}}$ (Å^3)	83.7(2)	82.3(4)	55.9(7)	81.8(5)	10(2.3)
Channel [100]					
O1-O1$_{8\text{-ring}}$ (Å)	4.73(2)	4.65(4)	4.54(6)	4.74(4)	
O3-O3$_{8\text{-ring}}$ (Å)	2.79(3)	2.40(2)	2.44(4)	2.73(3)	
$V_{ch\ 8\text{-ring}}$ (Å^3)	164.4(3)	149.9(4)	132.9(3)	161.7(2)	18(1.5)

* data collected under room conditions after compression.

The position of the extra-framework cations (in CS1 and CS2 sites) and water molecules (in W1, W2, W3, W4, W5, W6 sites) was almost maintained within the pressure range investigated (Table 3). However, looking in more detail at the evolution of the extra-framework bond distances reveals a different behaviour between CS1 and CS2. In the 10-ring channel, both the CS1-framework oxygen distances and the CS1-water molecule distances decreased with pressure, and on the whole the configuration remained the same as observed under room conditions. In the [001] 8-ring channel, on the contrary, the O1 moved towards the inside and as a consequence the distances between CS2 and O1 decreased from 2.533(8) Å to 2.27(6) Å, as the pressure increased to 3.4 GPa. At the same time, the distances between CS2 and the water molecule oxygens (CS2-W3, CS2-W3', CS2-W4, see Table 5) increased slightly with pressure.

Amorphization

Significant peak broadening, interpreted as an indication that amorphization was occurring, was observed at *P* higher than 3.7 GPa. At 4.1 GPa the peak disappearance hindered the determination of the lattice parameters. The evolution of the diffraction pattern during decompression showed that the gradual transition to the amorphous phase was still reversible, at least in the range 0.0001-5 GPa. A similar effect was observed for scolecite after complete H*P*-amorphization at 8-9 GPa (Gillet *et al.*, 1996) and for α-$AlPO_4$ (Gillet *et al.*, 1995).

The structural refinement under room conditions, after the H*P* measurements, showed little difference from the initial values of the lattice parameters and structural geometry (Tables 3-5).

Discussion and conclusions

Heulandite represents the first example of zeolite studied under pressure using single-crystal X-ray diffraction data. With this method the path followed by polyhedral tilting to deform the structure may be examined in detail. In particular the evolution of the lattice parameters may be understood by means of high-pressure structural refinements. Although the heulandite structure could be considered to be a layer structure packed along [010], where dense silicate layers alternate with 10- and 8-ring channels (Fig. 1), the largest compressibility we observed was along the *a* axis, not along the *b* axis. This apparently anomalous behaviour was due to the counter-balancing effect of two mechanisms: first the kinking of the zig-zag FPU chains, that increases the [010] layer thickness, and second the compression of the channels along [010]. On the other hand, along the *a* axis the two mechanisms act in the same way: both the kinking of the zig-zag FPU chains and the decrease of the channel size reduce the *a* axis, which was the most compressible lattice parameter.

However, in the heulandite structure the most compressible direction, as found by the strain analysis, does not coincide with any of the lattice parameters but lies in the (010) plane forming an angle of about 35° with the *a* axis. This direction corresponds approximately to the [102] axis along

Table 5. Interatomic distances (Å) in function of pressure.

P (GPa)	0.0001	1.45	3.4	0.0001*
CS1-O2 (x2)	2.695(6)	2.70(4)	2.65(5)	2.705(6)
CS1-O3 (x2)	3.089(5)	2.88(4)	2.92(4)	3.058(6)
CS1-W1	2.478(1)	2.42(3)	2.37(3)	2.475(11)
CS1-W2	2.399(23)	2.36(5)	2.24(5)	2.393(20)
CS1-W5 (x2)	2.922(12)	2.78(8)	2.72(6)	2.945(9)
CS1-W6	2.575(20)	2.35(5)	2.33(4)	2.573(20)
CS2-O1	2.533(8)	2.56(4)	2.27(6)	2.541(8)
CS2-O10 (x2)	2.712(6)	2.75(5)	2.83(5)	2.707(6)
CS2-W3 (x2)	2.403(8)	2.37(5)	2.39(6)	2.408(8)
CS2-W3' (x2)	2.576(9)	2.73(4)	2.76(6)	2.553(9)
CS2-W4	2.605(6)	2.62(2)	2.71(4)	2.633(5)
CS2-CS2	2.693(10)	2.42(4)	2.04(7)	2.672(9)
T1-O3	1.629(5)	1.63(3)	1.57(3)	1.636(5)
T1-O4	1.636(5)	1.63(4)	1.69(5)	1.637(5)
T1-O6	1.646(4)	1.64(2)	1.65(2)	1.634(4)
T1-O9	1.620(6)	1.70(6)	1.56(5)	1.628(5)
<T1-O>	1.632	1.65	1.62	1.634
T2-O1	1.647(2)	1.61(3)	1.58(2)	1.644(2)
T2-O2	1.665(5)	1.65(3)	1.72(3)	1.660(5)
T2-O4	1.654(5)	1.63(2)	1.69(2)	1.656(5)
T2-O10	1.665(5)	1.66(3)	1.75(4)	1.663(5)
<T2-O>	1.658	1.64	1.68	1.656
T3-O2	1.635(5)	1.59(5)	1.59(5)	1.629(5)
T3-O3	1.642(5)	1.69(3)	1.66(3)	1.628(5)
T3-O7	1.635(5)	1.64(4)	1.68(4)	1.623(5)
T3-O9	1.635(6)	1.63(4)	1.63(4)	1.637(5)
<T3-O>	1.637	1.64	1.64	1.629
T4-O5	1.636(3)	1.63(3)	1.68(4)	1.634(3)
T4-O7	1.594(5)	1.53(5)	1.50(5)	1.614(5)
T4-O8	1.626(5)	1.58(3)	1.65(3)	1.624(5)
T4-O10	1.635(5)	1.62(5)	1.54(5)	1.628(5)
<T4-O>	1.623	1.59	1.59	1.625
T5-O6 (x2)	1.638(5)	1.72(3)	1.65(3)	1.667(5)
T5-O8 (x2)	1.620(5)	1.66(4)	1.58(4)	1.636(5)
<T5-O>	1.629	1.69	1.61	1.651

* data collected under room conditions after compression.

which the FPU chains extend and where the diagonal of the system of channels lies along [100] and [001] (Fig. 3). The most compressible direction is likely to be related to the FPU tilting, mainly acting where the charge density is lower, as along the channel system diagonal.

The high-pressure behaviour of heulandite may be compared with the high-temperature behaviour described by Alberti & Vezzalini (1983). In their study the authors described a phase transition over 250°C from heulandite A to heulandite B, a contracted completely dehydrated phase. The water loss determined a drastic deformation of FPU, with T-O-T bridge breaks yielding an interrupted framework. In our study, with the pressure increase the extra-framework content remained unchanged, both cations and water molecules maintained almost the same position and the same occupancy.

Thus the deformations induced by *P* are less dramatic than those affected by *T* and no phase transition was observed before amorphization. The reflection broadening observed for pressures greater than 3.7 GPa, can be ascribed to the gradual amorphization. The analysis of structural refinement data allows us to hypothesize the reason for structural decay. The compression of 10-ring channel along [010] pushes the O1 oxygen toward the inside of the adjacent 8-ring channel, strongly reducing the CS2-O1 distance (Table 5). At the same time the distance between T2-O1 also decreases greatly. Under room conditions the O1 oxygen is under-bonded, in fact it is the bridging oxygen between two tetrahedra where silicon is largely substituted by aluminium; with pressure increase, the distances between the tetrahedral cation, as well as those between extra-framework cations, drastically decrease and as a consequence this oxygen becomes overcharged. Because of the "delicate" role of the O1 oxygen, as (010) layer binder, the charge imbalance on it could possibly produce significant structural instability.

Acknowledgements: Thanks are due to G. Vezzalini and S. Quartieri for the sample and for the microprobe analysis, and to A. Alberti for the determination of Al-content in tetrahedral sites. The paper greatly benefited from their helpful comments and discussion. This work was financially supported by M.U.R.S.T. (project "Relations between structure and properties in minerals: analysis and applications").

References

Alberti, A. (1972): On the crystal structure of zeolite heulandite. *Tscherm. Miner. Petr. Mitt.*, **18**, 129-146.

– (1973): The structure type of heulandite B (heath-collapsed phase). *Tscherm. Miner. Petr. Mitt.*, **19**, 173-184.

Alberti, A. & Gottardi, G. (1988): The determination of Al-content in the tetrahedra of framework silicates. *Z. Kristallogr.*, **184**, 49-61.

Alberti, A. & Vezzalini, G. (1983): The thermal behaviour of heulandites: structural study of the dehydration of Nadap heulandite. *Tscherm. Miner. Petr. Mitt.*, **31**, 259-270.

–,– (1984): Topological changes in dehydrated zeolite: breaking of T-O-T oxygen bridges. *in* "Proc. 6th Int. Zeolite Conf. Reno.", Olson, D. & Bisio, A., eds., Butterworth, Guildford, U.K., 834-841.

Alberti, A., Quartieri, S., Vezzalini, G. (1994): Structural modifications induced by dehydration in yugawaralite.

in "Zeolite and related microporous materials: state of the art 1994". Studies in surface sciences and catalysis, Vol. **84**, Weitkamp, J., Karge, H.G., Pfefer, H., Holderich, W., eds., Elsevier Science B.V., 637-644.

Angel, R.J., Hazen, R.M., McCormick, T.C., Prewitt, C.T., Smith, J.R. (1988): Comparative compressibility of end-members feldspars. *Phys. Chem. Minerals*, **15**, 313-318.

Belitsky, I.A., Fursenko, B.A., Gabuda, S.P., Kholdeev, O.V., Seryotkin, Y.V. (1992): Structural transformation in Natrolite and Edingtonite. *Phys. Chem. Minerals*, **18**, 497-505.

Birch, F. (1978): Finite strain isotherm and velocities for single-crystal and polycrystalline NaCl at high pressures and 300 K. *J. Geophys. Res.*, **83**, 1257-1267.

Bresciani-Pahor, N., Calligaris, M., Nardin, G., Randaccio, L., Russo, E., Comin-Chiaromonti, P. (1980): Crystal structure of a natural and a partially Ag-exchanged heulandite. *J. Chem. Soc. Dalton Trans.*, **1980**, 1511-1514.

Comodi, P., Mellini, M., Zanazzi, P.F. (1990): Scapolites: variation of the structure with pressure and possible role in the storage of fluids. *Eur. J. Mineral.*, **2**, 195-202.

Comodi, P. & Zanazzi, P.F. (1993): Improved calibration curve for the Sm^{2+}: BaFCl pressure sensor. *J. Appl. Cryst.*, **26**, 843-845.

Denner, W., Schulz, H., d'Amour, H. (1978): A new measuring procedure for data collection with high-pressure cell on X-ray four-circle diffractometer. *J. Appl. Cryst.*, **11**, 260-264.

Finger, L.W. & King, H. (1978): A revised method of operation of the single-crystal diamond cell and refinement of the structure of NaCl at 32 kbar. *Am. Mineral.*, **63**, 337-342.

Gillet, P., Badro, J., Varel, B., McMillian, P.S. (1995): High pressure behaviour in α-$AlPO_4$: Amorphization and the "Memory Glass" effect revisited. *Phys. Rev.*, **B51**, 11262-11269.

Gillet, P., Malézieux, J.M., Itié, J.P. (1996): Phase changes and amorphization of zeolites at high pressure: The case of scolecite and mesolite. *Am. Mineral.*, **81**, 651-657.

Hazen, R.M. & Finger, L.W. (1979): Polyhedral tilting: a common type of pure displacive phase transition and its relationship to analcite at high pressure. *Phase Transitions*, **1**, 1-22.

–,– (1984): Compressibility of zeolite 4A is dependent on the molecular size of the hydrostatic pressure medium. *J. Appl. Phys.*, **56**(6), 1838-1840.

Ibers, J.A. & Hamilton, W.C., eds. (1974): International tables for X-ray crystallography, vol. **IV**, Kynoch, Birmingham, U.K.

Jones, J.B. (1968): Al-O and Si-O tetrahedral distances in aluminosilicate framework structures. *Acta Cryst.*, **B24**, 355-358.

Mortier, W.J. & Pearce, J.R. (1981): Thermal stability of the heulandite-type framework: crystal structure of the calcium/ammonium form dehydrated at 483 K. *Am. Mineral.*, **66**, 309-314.

Mumpton, F.A. (1988): Development of uses for natural zeolites: A critical commentary. *in* "Occurrence, properties and utilization of natural zeolites", Kallo D. & Sherry H.S., eds., Akademiai Kiado, Budapest, Hungary, 333-365.

North, A.C.T., Phillips, D.C., Mathews, F.S. (1968): A semiempirical method of absorption correction. *Acta Cryst.*, **A24**, 351-359.

Ohashi, Y. (1982): A program to calculate the strain tensor from two sets of unit-cell parameters. *in* "Comparative Crystal Chemistry", Hazen, R.M. & Finger, L.W., eds., Wiley, New York, 92-102.

Press, W.H., Flannery, B.P., Teukolsky, S.A., Vetterling, W.T. (1986): Numerical recipes. Cambridge University Press, Cambridge, U.K., 521-528.

Sheldrick, G.M. (1997): SHELX-97. Programs for crystal structure determination and refinement. Institut für Anorg. Chemie, Univ. of Göttingen, Germany.

Smyth, J.R. (1982): Zeolite stability and radioactive waste isolation in volcanic rocks. *J. Geol.*, **90**, 195-201.

Utada, M. (1970): Occurrence and distribution of authigenic zeolites in the Neogene pyroclastic rocks in Japan. *Sci. Papers, College of General Education, Univ. of Tokyo*, **20**, 191-262.

Vaniman, D.T. & Bish, D.L. (1993): The importance of zeolite in the potential high-level radioactive waste repository at Yucca Mountain, Nevada. *in* "Natural Zeolites '93", Ming, D.M. & Mumpton, F.A., eds., Int. Comm. Natural Zeolites, Brockport, New York, 533-546.

Vezzalini, G., Quartieri, S., Alberti, A. (1993): Structural modifications induced by dehydration in the zeolite gismondine. *Zeolites*, **13**, 34-42.

Received 12 June 2000
Modified version received 16 October 2000
Accepted 2 January 2001